Journal of Magnetism and Magnetic Materials 496 (2020) 165915

Contents lists available at ScienceDirect

Journal of Magnetism and Magnetic Materials

journal homepage: www.elsevier.com/locate/jmmm

Research articles

Physical properties of Ruddlesden-Popper (n = 3) nickelate: $La_4Ni_3O_{10}$

Susmit Kumar*, Øystein Fjellvåg[1], Anja Olafsen Sjåstad, Helmer Fjellvåg*

Centre for Materials Science and Nanotechnology, Department of Chemistry, University of Oslo, P.O. Box 1033, N-0315 Oslo, Norway

ARTICLE INFO

Keywords:
Ruddlesden-Popper
Nickelates
Quasi-2D
Pauli paramagnetic
Charge density waves

ABSTRACT

Nickelates, just like their isoelectronic cousins (the cuprate superconductors), are candidates for high temperature superconductivity. As charge density waves (CDW) and superconductivity might share a similar microscopic origin and that CDW behaviour is earlier suggested for $La_4Ni_3O_{10}$, we here provide a detailed physical characterization of the magnetic, electronic and thermodynamic properties of stoichiometric polycrystalline $La_4Ni_3O_{10}$ at and below 300 K. By variable temperature, synchrotron powder X-ray diffraction, we observe noticeable expansion in the b-axis and a contraction in c-axis coinciding with the electronic transition. Magnetic measurements indicate Pauli paramagnetic behaviour for the entire temperature range of 4–300 K. Transport data suggest electron–phonon interaction based conduction from 150 to 300 K, at 138 K the we observe an anomaly of second order nature, previously reported as a CDW anomaly. Below this anomaly, we observe no indications of electron–phonon interaction, but rather, Fermi liquid (FL) based T^2 dependence with resistivity minima at 20 K, below which $T^{1/2}$ dependence occurs for the resistivity indicating pure electron–electron interactions (EEI) based transport. Specific heat data indicates that mass enhancement of $La_4Ni_3O_{10}$ similar to that of the normal state of the cuprates and the entropy change at anomaly suggests close similarities to other quasi-two dimensional systems, such as molybdenum bronzes and manganites.

1. Introduction

Charge density wave (CDW) transitions generally occur in low dimensional, highly anisotropic solids. In such systems, it is possible to achieve the nesting of the Fermi surfaces leading to creation of lattice distortions that are of periodic nature and result in the creation of an energy gap. This was first proposed by Rudolph Peierls for quasi-one-dimensional solids, and later theoretically demonstrated by Herbert Fröhlich [1,2]. (Quasi) Two – and three –dimensional CDW systems are attracting attention as they directly compete with superconductivity in high – Tc superconducting cuprates [3,4]. Since mid-1970s, numerous quasi-one-dimensional and two-dimensional metals showing CDW state are studied. Some examples are $K_2Pt(CN)_4$ $Br_{0.3}.3.2D_2O$ (KCP) [5,6], blue [7] and purple bronzes [8] and references therein, quasi-1D transition metal trichalcogenides [9], quasi-2D transition metal dichalcogenides [10,11], rare-earth tellurides [12], and strongly correlated electron systems such as manganites [13], cuprates [14], nickelates [15] and cobaltites [16]. Recently, these systems are re-visited due to a deeper understanding of how static CDW order at long-range appears to compete with BSC-type of superconductivity [17]. Short-range correlations exist over substantial range of carrier concentrations, supporting the appearance of superconductivity [18], which in turn suggests that both these situations might share a common microscopic origin [19].

Purple molybdenum bronzes $A_{0.9}Mo_6O_{17}$ (A = Li, Na, K and Ti) underwent careful studies in the 1980s [8]. For $K_{0.9}Mo_6O_{17}$ (space group $P\bar{3}$), Mo atoms are located in 2D slabs of octahedra, structurally similar to monoclinic Mo_4O_{11} [7,8]. The compound shows an unconventional CDW state at its surface that is not driven by electron–phonon coupling (EPC), but rather by strong electron–electron correlations [20]. Interestingly, transport and specific heat measurements [21] on single crystals shows unexpected similarities to the behaviour of the currently investigated $La_4Ni_3O_{10}$ nickelate system.

Nickelates of the Ruddlesden-Popper (RP) type [22] that can be isoelectronic to Cu-based superconductors [23], and have faced a resurging interest since the revisiting of the reduced $La_4Ni_3O_8$ phase in 2010 [24] and $Pr_4Ni_3O_8$ phase in 2017 [25]. At the same time, research is focused towards deeper understanding of the parent perovskite type oxides, for instance in thin-films for applications in oxide heterostructures and electronics [26]. Several publications describe in detail the properties of RP-1 (n = 1), RP-2 (n = 2) and RP-3 (n = 3) phases of $La_{n+1}Ni_nO_{3n+1}$ [24]. This includes pressure dependent resistivity and

* Corresponding authors.
E-mail addresses: susmit.kumar@kjemi.uio.no (S. Kumar), helmer.fjellvag@kjemi.uio.no (H. Fjellvåg).
[1] Present address: Department of Physics, Institute for Energy Technology (IFE), Instituttveien 18, NO-2007 Kjeller, Norway.

https://doi.org/10.1016/j.jmmm.2019.165915
Received 9 July 2019; Accepted 28 September 2019
Available online 28 September 2019

specific heat measurements [27] and angle resolved photoemission spectroscopy (ARPES) measurements on single crystals of $La_4Ni_3O_{10}$ [28]. The latter study suggest the existence of hole-pockets resembling a cuprate-hole Fermi surface, and describes similarities in electronic structure and dynamics of nickelate and cuprate systems. The ARPES data indicated a $d_{3z^2-r^2}$ band with opening of a low temperature energy gap of 20 meV that coincide with a metal-to-metal electronic transition observed in transport measurements. Puggioni and Rondinelli in their 2018 paper suggested that the electronic phase transition to be structural in nature, possibly transitioning from a high temperature monoclinic $P2_1/a$ phase (Z = 4) to a smaller volume low temperature $P2_1/a$ phase (Z = 2) [29].

We currently present detailed characterisation of polycrystalline samples of $La_4Ni_3O_{10}$ using structural, magnetic, transport and specific heat measurements. By means of low temperature (LT) synchrotron powder X-ray diffraction (SR-PXRD), we identify a noticeable expansion in the b-axis and a contraction in c-axis coinciding with the electronic transition. Magnetic data shows Pauli-paramagnetic behaviour for the entire temperature range from 4 to 300 K, whereas transport and magneto-transport measurements shows electron–phonon interactions causing a linear temperature dependence in resistivity from 150 to 300 K, below which the system transitions with an abrupt increase in resistivity of ≈2–3%. On further lowering of temperature the system transition into T^2 dependence for the resistivity. We provide further magneto-transport data show strong field dependence in resistivity as a function of temperature and a positive magnetoresistance of ≈1.6% at 4 K. Finally, specific heat data are reported for the entire temperature range (4–300 K). This paper lays the groundwork for subsequent works on even more detailed studies of the electronic instability in $La_4Ni_3O_{10}$ by both theory and experiments.

2. Material and methods

Powders of $La_4Ni_3O_{10}$ were synthesized using the citric acid method as reported in [33] with La_2O_3 (99.99%, Molycorp), Ni $(CH_3COO)_2{\cdot}4H_2O$ (≥99.0%, Sigma Aldrich), citric acid monohydrate, $C_3H_4(OH)(COOH)_3{\cdot}H_2O$ (98%, Sigma Aldrich) and HNO_3 (68% VWR Chemicals) as reactants. Metal precursors were dissolved at acidic conditions and complexed with citric acid before drying at 180 °C and calcination at 450 °C for 24 h. Obtained powders were cold pressed and annealed for 48 h at 1000–1100 °C in static air, and similarly re-annealed after intermediate grinding and re-pelletizing. Cold-pressed pellets for transport and heat capacity measurements were finally annealed for 48–96 h at 1000–1100 °C in static air.

Low temperature synchrotron powder XRD data were measured at BM01 (Swiss-Norwegian Beamlines, SNBL) at ESRF in Grenoble, France, at a wavelength of λ = 0.71490 Å and using a 2D PILATUS2M detector [30]. The carefully grinded powder sample was filled into a 0.3 mm diameter borosilicate capillary. Samples were cooled using an Oxford Cryostream 700+ nitrogen blower and powder diffraction patterns were collected between 100 and 300 K at a detector distance of 300 mm. The 2D images were integrated using the SNBL Bubble software to provide rebinned 1D diffraction patterns from $0 < 2\theta < 34.8^\circ$ with a step size of 0.01°. The patterns were simultaneously refined in a surface refinement in the TOPAS V5 software [31] to the same crystal structure where unit cell parameters were refined for each individual scan. Stephens model for anisotropic broadening in powder diffraction was used and refined to all scans simultaneously [32].

Magnetic property, resistivity and specific heat data were measured using a Quantum Design® Physical Property Measurement System (PPMS) using the DC Susceptibility, DC Resistivity, Electro-transport and Specific Heat Capacity options for the temperature range 2–300 K. All samples for DC magnetization measurements were held in gelatine capsules and studied under both zero field cooled (ZFC) and field cooled (FC) conditions, where, measurements were made during warming for applied fields of up to 9 T. DC resistivity data were measured on rectangular pellets of known area. Four-wire electrical connections were mounted to the rectangular pellets for connecting to the DC Resistivity insert. Gold wires were used for electrical connections with the silver paste. A battery of magneto-resistance measurements were performed as function of temperatures (4–300 K) and applied magnetic field of up to 9 T. For specific heat measurements, the pellets were broken into smaller pieces and placed on top of the alumina sample holder with Apizon N thermal contact grease to ensure good quality contacts. Measurements were carried out at constant pressure (C_P) in the 2–300 K temperature range with and without applied magnetic field of up to 9 T. Prior to C_P (T, B) measurements, the puck was calibrated for the 1.8–400 K range and addenda calibration was carried out with Apizon N grease in the 2–300 K region. Subsequently, low temperature magnetic field calibrations were carried out.

3. Results and discussion

3.1. Crystal structure

The current Rietveld profile refinement of the high-resolution temperature dependent X-ray diffraction (SR-PXRD) data, clearly indicates that the crystallographic symmetry of $La_4Ni_3O_{10}$ is monoclinic (Z = 4; space group $P2_1/a$) in the temperature interval $100 \leq T \leq 300$ K; Fig. 1. The theoretical work by Puggioni and Rondinelli considered four possible polymorphs of $La_4Ni_3O_{10}$ with just slight differences in the atomic arrangement, but with different symmetries; i.e Bmab, Pcab and $P2_1/a$ (Z = 2). Different from $La_4Co_3O_{10\pm\delta}$, that may slightly oxidize and dissolve additional oxygen anions in the rock salt layer of the RP3 structure, $La_4Ni_3O_{10}$ has ideal stoichiometry, as proved by cerimetric titrations [33]. Hence, in $La_4Ni_3O_{10}$ nickel is formally present as Ni^{2+} and Ni^{3+} with an average oxidation state of 2.67. Earlier works have not found any indications for charge ordering in $La_4Ni_3O_{10}$ at room temperature.

The detailed analysis of the diffraction data reveals an anomaly near T ≈ 138 K, i.e., at the temperature where a distinct bump is observed in the resistivity (Fig. 2c). No additional diffraction peaks, nor peak

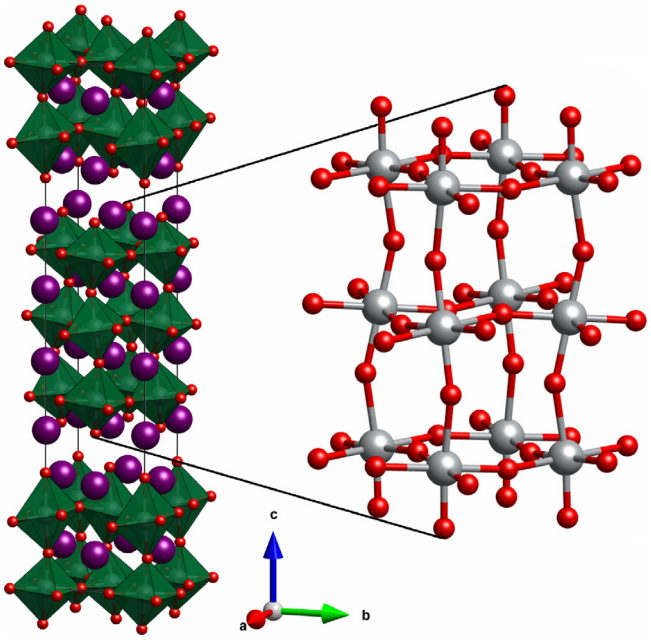

Fig. 1. The Ruddlesden-Popper (n = 3) $La_4Ni_3O_{10}$ crystal structure with monoclinic symmetry ($P2_1/a$ space group) where nickel (grey), lanthanum (violet) and oxygen (red) shown. (For interpretation of the references to colour in this figure legend, the reader is referred to the web version of this article.)

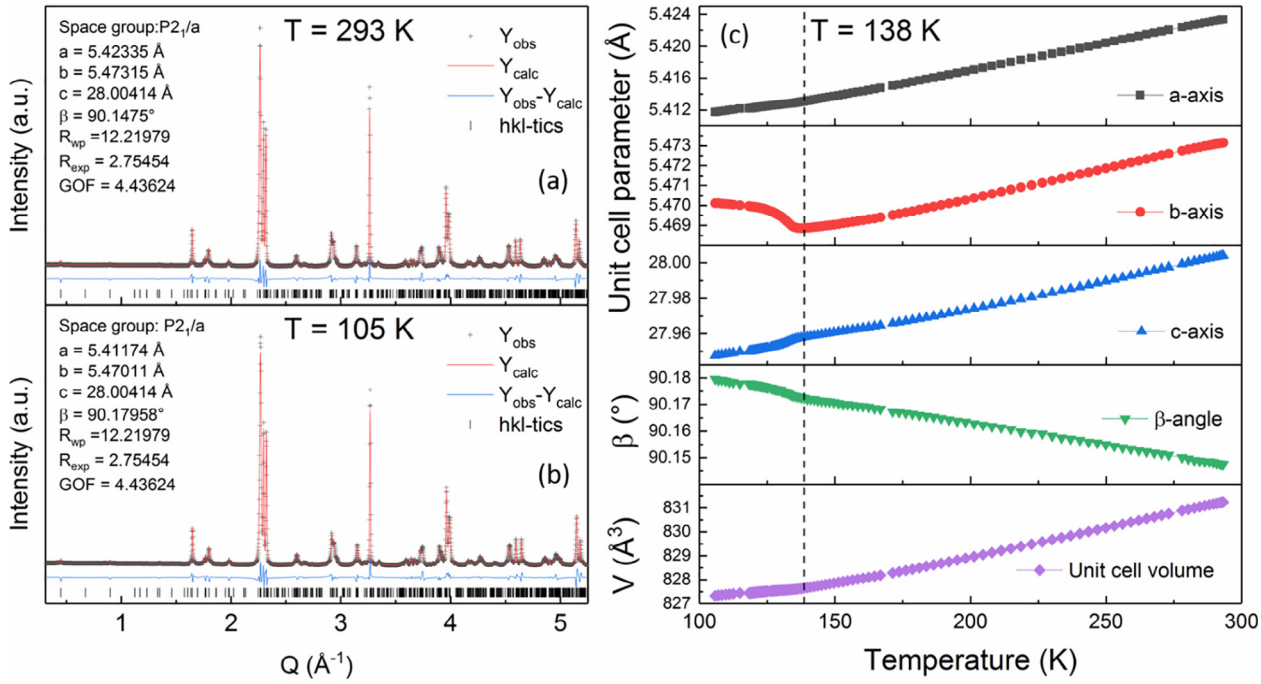

Fig. 2. The refined Rietveld profiles of selected temperature variable powder synchrotron X-ray diffraction data for $La_4Ni_3O_{10}$ at 293 (a) and 105 K (b); (c) variation of unit cell dimensions between 100 and 300 K.

splitting could be identified below the transition (Fig. 2a, b). We observe temperature dependent expansion of the unit cell dimensions with a linear volume expansion coefficient, $\alpha_{V1} \approx 2.48 \times 10^{-2}$ (K^{-1}) for the temperature region 190–300 K and linear volume expansion coefficient, $\alpha_{V2} \approx 2.02 \times 10^{-2}$ (K^{-1}) for 140–190 K. At $T_\lambda \approx 138$ K, we note a clear change taking place in all unit cell dimensions with a noticeable expansion of the b-axis. These changes are small (b ≈ 0.02%) and continuous, indicating a second order transition and could only be resolved based on high quality synchrotron data and/or temperature dependent electron diffraction studies. We carefully considered the possibility of having a transition into one of the other proposed polymorphs, Bmab, Pcab and P2$_1$/a (Z = 2), however, no such evidence were supported by Rietveld refinements of the current synchrotron data. For a detailed analysis of changes in interatomic distances, high-resolution powder neutron diffraction would be required. Our SR-XRD data nevertheless proves that the electronic transition is connected with structural changes, and hence, charge re-ordering due to electron–electron interactions are likely to be pronounced. It should be noted that for compounds like $NbSe_3$ and $NbSe_2$ the crystal structure remains within the resolution of X-ray diffraction unchanged above and below the electronic anomaly [34,35]. Techniques like pair distribution function (PDF) analysis of neutron total scattering data, variable temperature electron diffraction (ED), and resonant inelastic/elastic X-ray spectroscopy (RIXS/REXS) may help probe the delicate variations of structure and Fermi surface around the transition temperature.

3.2. Magnetism

$La_4Ni_3O_{10}$ is a weak Pauli paramagnet for the entire 4–300 K range, with a weak minimum in susceptibility at ≈90 K and weak temperature dependent behaviour further below (Fig. 3a). This observation is in line with our previous findings [33]. It is interesting to note the similarity to $A_{0.9}Mo_6O_{17}$ (A = Li, Na, K) that also shows Pauli paramagnetic behaviour. For A = K, strongly anisotropic susceptibility minimum is reported at ≈70 K, while a transition minimum at around 30 K points towards onset of a spin density wave (SDW). Quite similar behaviour was also observed for A = Na [8]. Noticeably, $La_4Ni_3O_{10}$ shows a magnetic field dependence at temperatures below the anomaly (see inset in Fig. 3a), with sharpening of the maximum in the susceptibility curve at ≈100 K and a quite hump-like variation at 9 T. This magnetic field dependent hump-like feature transitions into a strongly temperature dependent regime T < 50 K. The specific heat measurements (see specific heat section) indicates a high density of states (DOS) near the Fermi level, leading us to suggest that $La_4Ni_3O_{10}$ may be Stoner enhanced (Coulomb interactions enhanced) causing spontaneous weak itinerant magnetism, which would explain quadratic fit to $\rho = \rho_0 + BT^2$ Fermi liquid like dependence in resistivity, Fig. 3b (described in detail in following section). Just like $La_4Ni_3O_{10}$, the $La_2NiO_{4+\delta}$ system satisfies the Stoner criterion where $\alpha_0 \equiv I\,D(E_F) > 1$ [36]. The fact that there appears no anomalies at $T_\lambda \approx 138$ K in the susceptibility measurements, Fig. 3a, suggests a purely charge based picture for the presence of the anomaly.

3.3. Transport

The current thorough resistivity measurements for $La_4Ni_3O_{10}$, Fig. 3b, are fully in-line with previous reports on a metal-to-metal transition at ≈138 K that Goodenough et al. described as a charge density wave (CDW) behaviour [22]. Further to previous findings, we observe that the room temperature (300 K) resistivity of $La_4Ni_3O_{10}$ of ≈11,866 μΩ-cm is two orders of magnitude higher than its parent perovskite compound, the strongly correlated $LaNiO_3$ at ≈225 μΩ-cm [37]. The resistivity, ρ(T), for $La_4Ni_3O_{10}$ follows a linear temperature dependence, $\rho = \rho_0 + AT$, similar to what is seen in high-Tc cuprate superconductors, for the range 150–300 K that is below the calculated Debye temperature (θ_D). The electron–phonon coupling constant (Mc-Millan e-ph constant) is given by the expression, $1 + \lambda = (\gamma_{meas}/\gamma_{calc}) = 0.246(\hbar\omega_P)^2 A$, where $\hbar\omega_P$ is the plasmon energy (≈1 eV) [38], γ_{calc} the calculated Sommerfield constant, γ_{meas} the measured Sommerfield constant, and A is the slope of ρ(T). The calculated Mc-Millan e-ph coupling constant is 1 + λ ≈ 1.124 (λ = 0.124) indicating e-ph coupling approximately half of the reported value for $LaNiO_3$ (with λ ≈ 0.3), which suggests a weaker coupling between electrons and phonons [39]. The Debye temperature for $La_4Ni_3O_{10}$ is reported as ≈256 K [27], however, we currently find a higher Debye temperature of $\Theta_D \approx 384$ K, indicating strong phonon assisted metallic

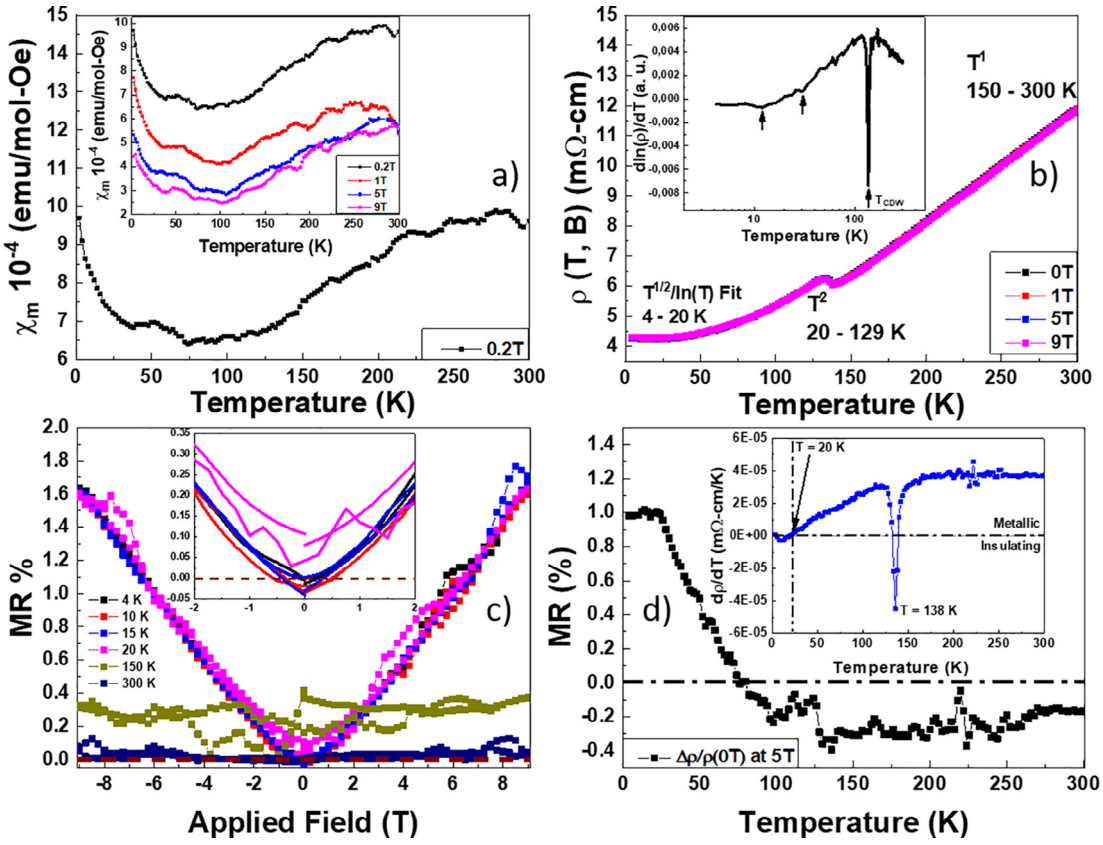

Fig. 3. Physical characterization data for $La_4Ni_3O_{10}$; (a) magnetic susceptibility measured in a field of 0.2 T; (b) Resistivity measured in fields of 0, 1, 5 and 9 T between 4 and 300 K; inset shows derivative curve of natural log of resistivity. (c) Magnetoresistance (MR %) at selected temperatures for applied fields for ± 9 T. (d) Ttemperature dependent MR calculated using **MR**(%) = $(\Delta\rho/\rho_0) \times 100$ where resistivity at 0 T and 5 T applied field were considered. T_{cross} = 76 K, shows the MR crossover temperature from negative to positive as the temperature is lowered. (d – Inset) Differential resistivity showing the saturation in the high temperature regime above the anomaly at $T_\lambda \approx 138$ K and drastic change of slope under eventually going negative.

conduction. With respect to room temperature, elastic scattering mean free path for electrons, $\ell_{min} = \nu_F\tau = (4.95 \times 10^{-4} v_F/(\rho(\hbar\omega_P)^2)$, where ν_F is Fermi velocity and τ is relaxation time, we get $\ell_{min} \approx 16.9$ Å. This corresponds to a mean free path greater than the unit cell dimension in the a-b plane (≈5.4 Å), however, substantially less than the c-axis unit cell distance (c ≈ 28 Å) reaffirming that conduction being localized in 2-dimensions for $La_4Ni_3O_{10}$. This elastic mean free path value is half the value for the polycrystalline parent compound $LaNiO_3$ (≈31 Å) at 300 K, and substantially smaller than metal Cu (≈390 Å) [39–41]. From free-electron model, we obtain $k_F\ell \approx 0.129$ at 300 K [38], where k_F is the Fermi wave vector, which is lower than the Ioffe-Regel criterion of $k_F\ell \approx 1$ for MIT, indicating presence of strong disorder in the system [42]. Finally, above the temperature of the anomaly of $T_\lambda \approx 138$ K, we find the positive temperature coefficient of resistivity $(1/\rho)(d\rho/dT)$ to vary from 2.94×10^{-3} K^{-1} at RT to 5.2×10^{-3} K^{-1} close to the anomaly. Whereas, below the anomaly of $T_\lambda \approx 138$ K until 20 K, there is a much sharper drop in the coefficient value to zero. Furthermore, below 20 K the system gives a negative temperature coefficient of resistivity $(1/\rho)(d\rho/dT)$, suggesting a possible metal-to insulator transition (MIT) [55].

As mentioned at the end of previous section, at temperatures below the transition, i.e., 20–130 K, a quadratic dependence $\rho = \rho_0 + BT^2$ is observed for the resistivity which is reminiscent of electron–electron scattering processes according to the Landau-Fermi liquid (LFL) theory for metals [43]. The fitted parameters are B ≈ 0.12836 μΩ-cm/K^2 and a residual resistivity of $\rho_0 \approx 4067.4$ μΩ-cm. Naito et al. reported a similar T^2 dependence for 2H-based transition metal dichalcogenide systems that were associated with both electron–electron scattering, as well as, collective excitations of the CDW that disturb the perfect order (electron-phason or electron-amplitude mode scattering) [44]. However, in their 2H-based transition metal dichalcogenide system, they also observed Bloch – Grüneisen T^5 dependence below the T^2 region (2H-$TaSe_2$) and a direct T^1 to electron – phonon scattering T^3 transition (2H-$NbSe_2$) on lowering the temperature. Whereas for $La_4Ni_3O_{10}$, around the anomaly at $T_\lambda \approx 138$ K, we observe a direct transition in temperature dependent resistivity from T^1 to T^2 as the temperature was lowered, with absence of any temperature regions with different dependencies till the resistivity minimum. This suggests an electron–electron scattering only picture rather than its combination with scattering of electrons due to CDW fluctuations (phonon entropy model). Further, below the anomaly at $T_\lambda \approx 138$ K, there is a possibility that electron localization leads to charge re-ordering, ultimately causing changes to the bond lengths and the b-lattice parameter change, as mentioned in previous section.

Field-dependent and temperature-dependent magnetoresistance (MR) measurements were carried out for $La_4Ni_3O_{10}$ in temperature ranges from 4 to 300 K (see Fig. 3c and d). No noticeable MR effects were observed at 300 K and 150 K, however, a positive MR of 1.7% was observed at 20, 15, 10 and 4 K. Additionally, temperature-dependent resistivity measurements at varying applied magnetic field were carried out and temperature dependent MR was calculated using $MR(\%) = (\Delta\rho/\rho_0) \times 100$, where resistivity at 0 T and 5 T applied field were considered for Δρ values (see Fig. 3d). A cross-over from high temperature negative MR to low temperature positive MR is observed at approximately $T_{cross} \approx 76$ K, which is also evident in temperature dependent MR curve. Coming back to aspect of positive MR observed from 4 to 20 K, it has been previously observed for $LaNiO_3$ parent compound and has been suggested to arise from band-like contribution as in

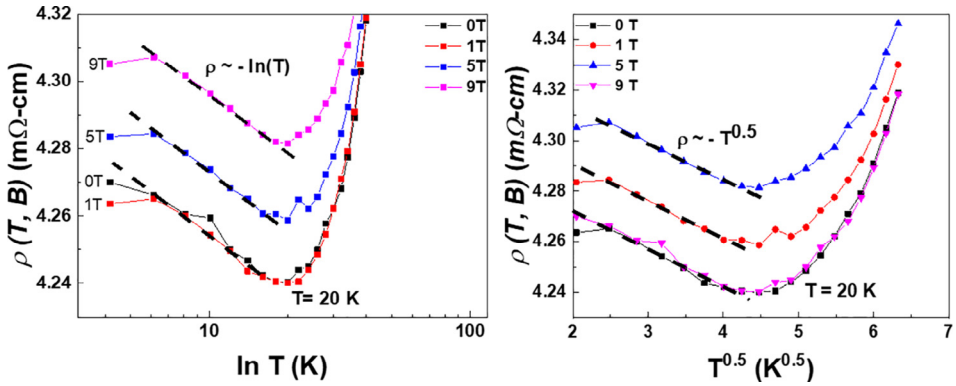

Fig. 4. Experimental low temperature resistivity data in the 4–20 K region (a) fitted with – ln(T) parameter associated with weak localization (WL); (b) fitted with – $T^{1/2}$ parameter associated with electron–electron interactions (EEI).

normal metals, however, of much larger magnitude [40]. According to theoretical calculations done by Altshuler et al., positive MR arises from spin splitting of conduction electron energies [48].

Various explanations exist for a resistivity upturn observed in $La_4Ni_3O_{10}$ at low temperatures (4–20 K), such as the non-Fermi liquid (NFL) behaviour. Such upturns have also been reported for $LaNiO_3$ both in bulk and as thin-films [45], as well as in manganites [46]. For Pauli paramagnetic $La_4Ni_3O_{10}$, two possibilities may explain the NFL behaviour, 1) weak localization (WL) effect due to finite dimensions of the system contribution to resistivity having – ln(T) dependence with presence of Kondo-like spin–orbit interactions, or 2) inelastic electron–electron interactions (EEI) having $-T^{1/2}$ dependence [47]. As we can see from Fig. 4, both $-T^{1/2}$ and -ln(T) dependence are equally applicable in the upswing region of resistivity below 20 K, indicating the presence of possibly both effects. Table 1 shows the extracted values of parameters for EEI, WL and T^2 dependence, the so-called Quantum Corrections to Conductivity (QCC) for the temperature range 4–130 K (also see Fig. 5). Both the residual resistivity and T^2 parameters show stable values when the magnetic field is applied from 1 to 9 T. However, in the case of EEI and WL, we observe complete suppression of WL effects and enhancement of EEI values, and the 9 T measurement gives anomalous values similar to when no magnetic field was applied. The data further suggests that the NFL region in the absence of applied magnetic field may be dominated by both WL and EEI effects. However, when the magnetic field is applied, we see complete suppression of WL effects and only EEI remain (see Table 1). This clearly indicate that the resistivity upswing in $La_4Ni_3O_{10}$ is a result of inelastic electron–electron interactions.

3.4. Specific heat

Specific heat measurements C_P (T, B) were carried out for the temperature ranges from 2 to 30 K with applied magnetic fields of 0 T ≤ B ≤ 9 T (Fig. 6b) and from 2 to 300 K without any applied magnetic field. Fig. 6a shows C_P(T) between 2 and 300 K (at 0 T). Detailed measurements were carried out in the range of the electronic transition (≈138 K) and values for the involved entropy changes were extracted (Fig. 6d). For the 2–8 K region (Fig. 6c), the linear specific heat dependence of C_P/T vs. T^2 signifies purely metallic conduction with possible electron–electron scattering. We note a clear change of slope at 8 K indicative of transitioning into a more complex scattering environment. By using the Sommerfield – Debye formula, $C_P(T) = \gamma T + \beta T^3$, for the 2–8 K region ($\gamma$ Sommerfield coefficient of electronic specific heat, β_3 Debye lattice (electron–phonon) specific heat coefficient) a good fit of the data was obtained for the values $\gamma \approx 15.53$ mJ/mol-K^2 and $\beta \approx 0.57$ mJ/mol-K^4, The Debye temperature Θ_D was calculated, $\theta_D = \{12\pi^4 rR/5\beta\}^{1/3}$, where r is the number of atoms in the unit cell and R the gas constant. The Debye temperature is comparable to what found for the parent $LaNiO_3$ perovskite ≈400 ± 20 K [49], and the quasi-2D KMo_6O_{17} system at 418 K, but,

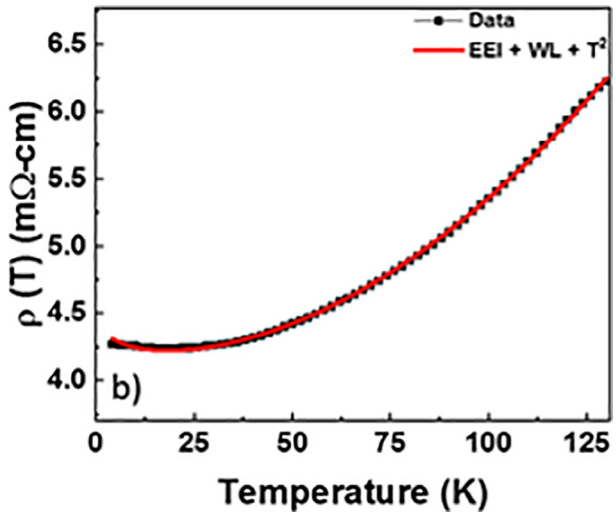

Fig. 5. Electron-electron interaction (EEI), weak localization (WL) and Fermi liquid fit of low temperature resistivity (ρ vs. *T*) data at zero applied field from 4 to 129 K. This temperature region is below the resistivity anomaly observed for $La_4Ni_3O_{10}$.

Table 1
Quantum corrections to conductivity values for $\rho = \rho_0 - \rho_{EEI}\, T^{1/2} + \rho_{WL}\, \ln(T) + \rho_{T^2}\, T^2$ where ρ_0 is the residual resistivity, ρ_{EEI} is due to strong electron-electron interactions in disordered systems at low temperatures, ρ_{WL} for systems with weak localization showing Kondo-like spin-orbit interactions. Also, related low temperature field dependent specific heat properties of $La_4Ni_3O_{10}$ are reported as well.

Sample LNO-RP3 4 < T < 130 K	ρ_0 (mΩ-cm/K)	$P_{EEI}\ 10^{-3}$ (mΩ-cm/$K^{1/2}$)	$P_{WL}\ 10^{-4}$ (mΩ-cm/lnK)	$P_{T^2}\ 10^{-5}$ (mΩ-cm/K^2)	Specific Heat T ≤ 8 K	Θ_D (K)	γ (mJ/mol K^2)
0 T	4.36	3.76	3.88	1.38	0 T	384	15.53
1 T	4.37	5.48	–	1.41	1 T	404	16.03
5 T	4.39	6.59	–	1.41	5 T	401	13.89
9 T	4.37	4.01	–	1.39	9 T	392	14.27

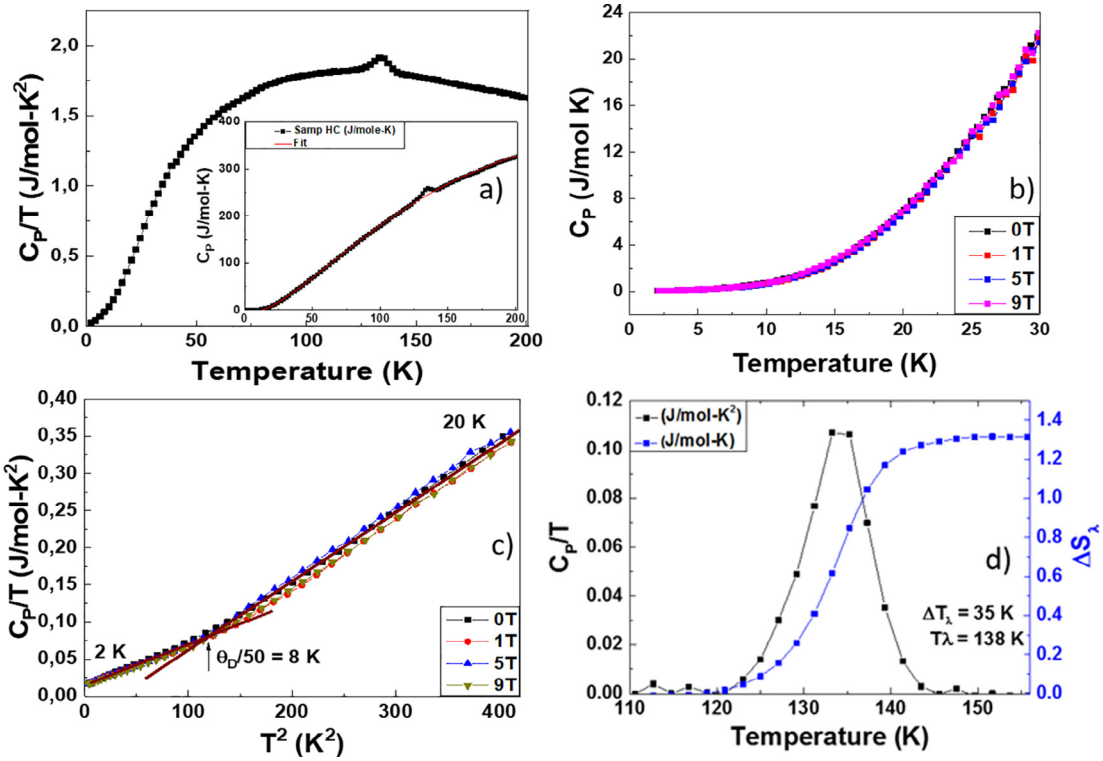

Fig. 6. (a) shows the constant pressure specific heat C_P/T vs. T for $La_4Ni_3O_{10}$ from 2 to 300 K in the absence of applied magnetic field demonstrating the smooth increase above the anomaly at 138 K and the sudden drop in specific heat below the anomaly. (inset) shows the measured specific heat and the polynomial fit to the data. (b) Shows the low temperature specific heat as a function of applied magnetic field. (c) Shows linear specific heat dependence of C_P/T vs. T^2 from 2 to 8 K that signifies purely electronic conduction with observable slope change around 10 K. (d) shows the specific heat extracted around the anomaly by subtracting the background using a polynomial fit and the resulting change in entropy across the anomaly.

slightly higher than for $K_{0.9}Mo_6O_{17}$ at 340 ± 10 K [50]. Also, the previously reported Debye temperature The density of states near the Fermi level $N(E_F)$ is estimated from Sommerfield coefficient $\gamma = \frac{\pi^2}{3}k_B^2 N(E_F)$, where k_B is the Boltzmann's constant, which gives a rather reasonable density of states near the Fermi level of 2.19 states eV^{-1} per formula unit of $La_4Ni_3O_{10}$ that is higher than reported values.

For the electron effective mass of $La_4Ni_3O_{10}$, Wu et al. obtained $m^*/m_0 \approx 2.56$. Currently we get a slightly lower but a comparable effective mass of $m^*/m_0 \approx 2.13$, closer to a normal metal than a strongly correlated such as $LaNiO_3$ with reported m^*/m_0 values of ≈9.38 and 15 [27,39]. Furthermore, the effective mass of $La_4Ni_3O_{10}$ is comparable to the normal state effective mass of cuprate systems [28,51–53], and is hence likely strongly influenced by electron-localization effects. Utilizing the Brinkman-Rice model for correlated electrons, where there is a direct correlation between effective mass of an electron m* and correlation energy U, using the expression $m^*/m_e = 1/[1 - (U/U_0)^2]$, we get correlation energy, $U \approx 0.73U_0$. This value suggests system to be metallic with presence of some density of states at the Fermi surface [42].

There is no hysteresis in the C_P vs T data at the transition $T_\lambda \approx 138$ K that suggests the anomaly to be of second order nature. The entropy (ΔS_λ) change was extracted from the data using a simple polynomial fit, Fig. 6x, showing a change of approximately ≈ 0.18 (R) or 0.5 J/mol-K or 0.06 (R) per Ni, where R is the gas constant. This value is comparable (possibly slightly larger) than the values reported for A-site calcium doped perovskite type manganites [13] and quite similar to values reported for the well-studied CDW system $K_{0.3}MoO_3$ with $\Delta S_{CDW} \approx 0.18$(R) [54]. $\Delta T_\lambda/T_\lambda$ is broad for the second order transition with a width of $\Delta T_\lambda \approx 35$ K, making it a wide cusp system with excess specific heat at transition to be $\Delta C_P/C_P \approx 6.32\%$. This lowering of energy compared to expected electronic contribution remains unclear, although, it may indicate some form of charge reordering.

4. Conclusions

In conclusion, we report in detail on the structural, magnetic, electronic and specific heat properties of $La_4Ni_3O_{10}$. According to temperature dependent SR-PXRD measurements, $La_4Ni_3O_{10}$ shows the same monoclinic $P2_1/a$ structure above and below the anomaly at 138 K. Magnetic measurements show a Pauli paramagnetic behaviour in the entire measured temperature range (2–300 K) with an observable increase in susceptibility at the lowest temperatures (2–20 K). The system remains metallic, with an exception for the resistivity upturn at ≈20 K, that may indicate electron localization due to observed strong logT and/or $T^{1/2}$ dependence in resistivity, or alternatively a density wave transition. Interestingly, we observe small positive magnetoresistance of ≈1.6% for T ≤ 20 K. Above 20 K, we also see a T^2 behaviour in resistivity until the anomaly, that could be either due to electron–electron interactions or just a by-product of transitioning through the anomaly. Above the anomaly, the system shows a phonon driven linear temperature (T^1) dependence (150–300 K) for the resistivity, similar to one observed for cuprate systems. Field dependent measurements show no changes to the linearity of the resistivity. Heat capacity measurements indicate a metallic nature of $La_4Ni_3O_{10}$ with effective mass of ≈2.13 and Debye temperature of θ_D = 384 K (0 T) similar to that observed for quasi-2D purple bronze systems. The resistivity and specific heat data indicate an electron–electron mediated conduction as the main driving force for entire temperature range below the anomaly. Definite confirmation of the nature of the anomaly will require combined use of advanced methods such as PDF analysis of neutron total scattering, electron diffraction or soft resonant inelastic/elastic X-ray spectroscopy techniques.

Acknowledgments

This work is part of activities in the NOFCO, FOXHOUND and NAMM projects. NOFCO and NAMM are supported by the Research Council of Norway (Grant no. 221905 and 263241 respectively), and FOXHOUND is funded by The Faculty of Mathematics and Natural Sciences, University of Oslo via the Strategic Research Initiative program. The authors acknowledge the staff at the Swiss-Norwegian Beam Lines (SNBL), ESRF, France, for technical support.

References

[1] R.E. Peierls, Quantum Theory of Solids, Oxford University Press, 1955.
[2] G. Gruner, Density Waves in Solids, Addison-Wesley, 1994.
[3] J. Chang, E. Blackburn, A.T. Holmes, N.B. Christensen, J. Larsen, J. Mesot, Ruixing Liang, D.A. Bonn, W.N. Hardy, A.V. Watenphul, M. Zimmermann, E.M. Forgan, S.M. Hayden, Nat. Phys. 8 (2012) 871.
[4] N. Mathur, F. Grosche, S. Julian, I. Walker, D. Freye, R. Haselwimmer, Nature 394 (6688) (1998) 39.
[5] J.W. Lynn, M. Iizumi, G. Shirane, S.A. Werner, R.B. Saillant, Phys. Rev. B 12 (4) (1975) 1154–1166.
[6] Y. Hu, F. Zheng, X. Ren, J. Feng, Y. Li, Phys. Rev. B 91 (14) (2015) 144502.
[7] J.P. Pouget, B. Hennion, C. Escribe-Filippini, M. Sato, Phys. Rev. B 43 (10) (1991) 8421–8430.
[8] M. Greenblatt, Chem. Rev. 88 (1) (1988) 31–53.
[9] C.W. Felser, E. Finckh, H. Kleinke, F. Rocker, W. Tremel, J. Mater. Chem. 8 (8) (1998) 1787–1798.
[10] J.A. Wilson, F.J. Di Salvo, S. Mahajan, Phys. Rev. Lett. 32 (16) (1974) 882–885.
[11] D.E. Moncton, J. Axe, F. DiSalvo, Phys. Rev. B 16 (2) (1977) 801.
[12] B.F. Hu, B. Cheng, R.H. Yuan, T. Dong, N.L. Wang, Phys. Rev. B 90 (8) (2014) 085105.
[13] S. Cox, J. Lashley, E. Rosten, J. Singleton, A. Williams, P. Littlewood, J. Phys. Condens. Matter 19 (19) (2007) 192201.
[14] J.M. Tranquada, B.J. Sternlieb, J.D. Axe, Y. Nakamura, S. Uchida, Nature 375 (1995) 561.
[15] C.H. Chen, S.W. Cheong, A.S. Cooper, Phys. Rev. Lett. 71 (15) (1993) 2461–2464.
[16] D. Qian, L. Wray, D. Hsieh, D. Wu, J.L. Luo, N.L. Wang, Phys. Rev. Lett. 96 (4) (2006) 046407.
[17] E.H. da Silva Neto, P. Aynajian, A. Frano, R. Comin, E. Schierle, E. Weschke, Science 343 (6169) (2014) 393.
[18] G. Ghiringhelli, M. Le Tacon, M. Minola, S. Blanco-Canosa, C. Mazzoli, N.B. Brookes, Science 337 (6096) (2012) 821.
[19] N.S. Sangeetha, A. Thamizhavel, C.V. Tomy, S. Basu, A.M. Awasthi, P. Rajak, Phys. Rev. B 91 (20) (2015) 205131.
[20] D. Mou, A. Sapkota, H.-H. Kung, V. Krapivin, Y. Wu, A. Kreyssig, Phys. Rev. Lett. 116 (19) (2016) 196401.
[21] X. Xu, A. Bangura, C. Niu, M. Greenblatt, S. Yue, C. Panagopoulos, Phys. Rev. B 85 (19) (2012) 195101.
[22] M. Greenblatt, Curr. Opin. Solid State Mater. Sci. 2 (2) (1997) 174–183.
[23] Bednorz JG, Müller KA. Nobel Prize in Physics in 1987, http://nobelprize.org.
[24] V.V. Poltavets, K.A. Lokshin, A.H. Nevidomskyy, M. Croft, T.A. Tyson, J. Hadermann, Phys. Rev. Lett. 104 (20) (2010) 206403.
[25] J. Zhang, A.S. Botana, J.W. Freeland, D. Phelan, H. Zheng, V. Pardo, Nat. Phys. 13 (2017) 864.
[26] G. Zhou, F. Jiang, J. Zang, Z. Quan, X. Xu, ACS Appl. Mater. Interfaces 10 (2) (2018) 1463–1467.
[27] G. Wu, J. Neumeier, M. Hundley, Phys. Rev. B 63 (24) (2001) 245120.
[28] H. Li, X. Zhou, T. Nummy, J. Zhang, V. Pardo, W.E. Pickett, Nat. Commun. 8 (1) (2017) 704.
[29] D. Puggioni, J.M. Rondinelli, Phys. Rev. B 97 (11) (2018) 115116.
[30] V. Dyadkin, P. Pattison, V. Dmitriev, D. Chernyshov, J. Synchrotron Radiat. 23 (2016) 825–829.
[31] Bruker-AXS TOPAS V5: General profile and structure analysis software for powder diffraction data, Bruker AXS, Karlsruhe, Germany., 2013.
[32] P. Stephens, J. Appl. Crystallogr. 32 (1999) 281–289.
[33] M.U. Nagell, S. Kumar, M.H. Sørby, H. Fjellvåg, A.O. Sjåstad, Phase Trans. 88 (10) (2015) 979–990.
[34] J. Hodeau, M. Marezio, C. Roucau, R. Ayroles, A. Meerschaut, J. Rouxel, J. Phys. C: Solid State Phys. 11 (20) (1978) 4117.
[35] M. Marezio, P. Dernier, A. Menth, G. Hull Jr, J. Solid State Chem. 4 (3) (1972) 425–429.
[36] T. Jarlborg, A. Bianconi, J. Supercond. Novel Magn. 29 (3) (2016) 615–621.
[37] A. Li, C. Ge, P. Lü, N. Ming, Appl. Phys. Lett. 69 (2) (1996) 161–163.
[38] M. Escote, V. Barbeta, R. Jardim, J. Campo, J. Phys.: Condens. Matter 18 (26) (2006) 6117.
[39] G.P. Mambrini, E.R. Leite, M.T. Escote, A.J. Chiquito, E. Longo, J.A. Varela, J. Appl. Phys. 102 (4) (2007) 043708.
[40] N. Gayathri, A.K. Raychaudhuri, X.Q. Xu, J.L. Peng, R.L. Greene, J. Phys.: Condens. Matter 10 (6) (1998) 1323.
[41] K.P. Rajeev, A.K. Raychaudhuri, Phys. Rev. B 46 (3) (1992) 1309.
[42] M. Hooda, C. Yadav, Phys. B 491 (2016) 31–36.
[43] M. Imada, A. Fujimori, Y. Tokura, Rev. Mod. Phys. 70 (4) (1998) 1039–1263.
[44] M. Naito, S. Tanaka, J. Phys. Soc. Jpn. 51 (1) (1982) 219–227.
[45] K. Sreedhar, J.M. Honig, M. Darwin, M. McElfresh, P.M. Shand, J. Xu, J. Spalek, Phys. Rev. B 46 (10) (1992) 6382–6384.
[46] G. Herranz, F. Sánchez, J. Fontcuberta, V. Laukhin, J. Galibert, M.V. García-Cuenca, Phys. Rev. B 72 (1) (2005) 014457.
[47] J. Androulakis, N. Katsarakis, Z. Viskadourakis, J. Giapintzakis, J. Appl. Phys. 93 (9) (2003) 5484–5490.
[48] B.L. Altshuler, A.G. Aronov, P.A. Lee, Phys. Rev. Lett. 44 (19) (1980) 1288.
[49] J.J. Hamilton, E.L. Keatley, H.L. Ju, A.K. Raychaudhuri, V.N. Smolyaninova, R.L. Greene, Phys. Rev. B 54 (21) (1996) 14926–14929.
[50] R. Buder, J. Devenyi, J. Dumas, J. Marcus, J. Mercier, C. Schlenker, J. Phys. Lett. 43 (2) (1982) 59–65.
[51] P.D. Johnson, T. Valla, A.V. Fedorov, Z. Yusof, B.O. Wells, Q. Li, Phys. Rev. Lett. 87 (17) (2001) 177007.
[52] T. Kim, A. Kordyuk, S. Borisenko, A. Koitzsch, M. Knupfer, H. Berger, J. Fink, Phys. Rev. Lett. 91 (16) (2003) 167002.
[53] A. Lanzara, P. Bogdanov, X. Zhou, S. Kellar, D. Feng, E. Lu, T. Yoshida, H. Eisaki, A. Fujimori, K. Kishio, Nature 412 (6846) (2001) 510–515.
[54] Y.K. Kuo, C.S. Lue, F.H. Hsu, H.H. Li, H.D. Yang, Phys. Rev. B 64 (12) (2001) 125124.
[55] M. Gurvitch, A.T. Fiory, Phys. Rev. Lett. 59 (12) (1987) 1337–1340.